Biomaterials 297 (2023) 122120

Contents lists available at ScienceDirect

Biomaterials

journal homepage: www.elsevier.com/locate/biomaterials

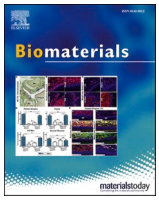

Nanocontroller-mediated dissolving hydrogel that can sustainably release cold-mimetic menthol to induce adipocyte browning for treating obesity and its related metabolic disorders

Ting Ruan [a,1], Chih-Yu Fu [b,1], Chih-Hung Lin [a,c,d], Kun-Chi Chou [a,b], Yu-Jung Lin [b,*]

[a] School of Medicine, College of Medicine, Fu Jen Catholic University, New Taipei City, Taiwan
[b] Research Center for Applied Sciences, Academia Sinica, Taipei, Taiwan
[c] Department of Internal Medicine, Cathay General Hospital, Taipei, Taiwan
[d] Ph.D. Program in Nutrition and Food Science, Fu Jen Catholic University, New Taipei City, Taiwan

ARTICLE INFO

Keywords:
Adipocyte browning
Metabolic disorder
Menthol
Cold senor
Injectable hydrogel

ABSTRACT

Obesity leads to the development of many metabolic diseases, causing severe health problems. Menthol can induce adipocyte browning and thus has been used to combat obesity. To deliver menthol with a sustained effect, an injectable hydrogel that comprises carboxymethyl chitosan and aldehyde-functionalized alginate that are crosslinked through dynamic Schiff-base linkages is developed to load menthol-cyclodextrin inclusion complexes (IC). To render the as-developed hydrogel soluble after its payload is released, amino acid-loaded liposomes, functioning as nanocontrollers, are covalently grafted onto networks of the hydrogel. Upon subcutaneous injection in mice with diet-induced obesity, the as-developed hydrogel absorbs body fluids and spontaneously swells, expanding and stretching its networks, gradually releasing the loaded IC. Menthol then disassociates from the released IC to induce adipocyte browning, triggering fat consumption and increasing energy expenditure. Meanwhile, the expanded hydrogel networks destabilize the grafted liposomes, which function as built-in nanocontrollers, unleashing their loaded amino acid molecules to disrupt the dynamic Schiff-base linkages, causing hydrogel to dissolve. The thus-developed nanocontroller-mediated dissolving hydrogel realizes the sustained release of menthol for treating obesity and its related metabolic disorders without leaving exogenous hydrogel materials inside the body, and thereby preventing any undesired adverse effects.

1. Introduction

The increasing prevalence of obesity is a serious health issue, affecting a considerable population globally [1]. Obesity, a chronic low-grade inflammatory condition, is strongly associated with the progression of numerous metabolic diseases, including type 2 diabetes and nonalcoholic fatty liver disease [2]. Current clinical approaches to tackling obesity include surgical intervention and the administration of appetite suppressants or fat absorption inhibitors [3]. However, surgical procedures, such as sleeve gastrectomy, are commonly accompanied by gastroesophageal reflux [4]; appetite suppressants sometimes cause dizziness, insomnia, and digestive problems; and fat absorption inhibitors reportedly induce nausea, indigestion, and steatorrhea [3]. These side effects may cause poor patient compliance. Accordingly, alternative approaches to weight management are urgently sought.

Obesity is a consequence of energy intake in excess of energy expenditure. The excess energy is stored as fats (mainly as triglycerides) in white adipocytes, resulting in fat accumulation within white adipose tissues (WAT) [5]. Numerous works have demonstrated that the sustained exposure of white adipocytes in WAT to cold may induce their transformation into brown-like adipocytes (beige adipocytes), a phenomenon known as “adipocyte browning” [6]. Unlike white adipocytes, which may function as energy depots, beige adipocytes are able to consume fats and generate heat in a process that is catalyzed by a thermogenic protein, mitochondrial uncoupling protein 1 (UCP1), potentially increasing energy expenditure [6]. Consequently, various strategies for converting white adipocytes into beige adipocytes for treating obesity and its related metabolic disorders have been studied

* Corresponding author.
E-mail address: linyujung@gate.sinica.edu.tw (Y.-J. Lin).
[1] The first two authors (T. Ruan and C. Y. Fu) contributed equally to this work.

https://doi.org/10.1016/j.biomaterials.2023.122120
Received 9 December 2022; Received in revised form 26 March 2023; Accepted 6 April 2023
Available online 10 April 2023

[7–9]. Among these, the cold-induced transformation of white adipocytes into beige adipocytes has attracted substantial research interest. However, in testing this strategy, test animals are typically housed at cold temperatures, so translating results to human beings is difficult [6,10,11].

Menthol reportedly activates the cold sensor of transient receptor potential melastatin subtype 8 (TRPM8) on white adipocytes to produce a sensation of cold [12]. Accumulating evidence demonstrates that a diet with menthol can trigger the browning of white adipocytes in mice, improving their metabolic activity, ultimately combating obesity [13–15]. The effect of menthol-induced adipocyte browning on diet-induced obese mice reportedly mimics that caused by exposure to cold. However, cold-mimetic menthol is a more acceptable treatment for human than is exposure to cold.

To render the effect of cold-mimetic menthol sustainable, an injectable hydrogel that comprises carboxymethyl chitosan (CMC) and aldehyde-functionalized alginate (AA) that are crosslinked through dynamic Schiff-base linkages is developed for loading and controlled release of cold-mimetic menthol (Fig. 1). A Schiff-base linkage (–C═N–) is typically formed by condensation between a primary amine ($–NH_2$) and an aldehyde group (–CHO) [16]. In this work, alginate is functionalized with aldehyde groups (AA) by oxidation of its hydroxyl groups, and then reacts with the primary amines on CMC, forming dynamic Schiff-base linkages, to yield a CMC-AA hydrogel. CMC and AA have been extensively used in the biomedical field because of their biocompatibility and biodegradability [17,18].

Menthol is lipophilic [19]. Direct incorporation of the poorly water-soluble menthol into a hydrophilic hydrogel matrix is challenging. To increase the efficiency of loading water-insoluble menthol in the hydrophilic hydrogel, cyclodextrin (CD) is used in the inclusion complexation of the lipophilic menthol [20]. CD, a cyclic polysaccharide, is derived from starch by enzymatic hydrolysis, and has been widely used as a drug carrier in the pharmaceutical industry [21]. CD has the shape of a truncated cone, whose hydrophobic interior offers a space to complex with lipophilic drug molecules, while its hydrophilic exterior surface renders the drug water-soluble [21].

An ideal hydrogel delivery system should be dissolved and adsorbed after releasing its payload, without leaving the exogenous hydrogel materials inside the body [22]. To make the as-developed hydrogel soluble, amino acid-loaded liposomes, functioning as nanocontrollers, are covalently grafted onto its networks. As the formation of a Schiff-base linkage may proceed reversibly, the coupling and uncoupling of the Schiff-base linkages in the hydrogel networks occur dynamically [23]. Therefore, an added amino acid, such as glycine, may compete with the amine groups on CMC to react with the aldehyde groups on AA to generate new Schiff-base linkages, resulting in dissolution of the CMC-AA hydrogel [24].

Fig. 1 displays the composition/structure of the nanocontroller-mediated dissolving hydrogel, the operating mechanism of the nanocontroller (amino acid-loaded liposome), and the therapeutic function of cold-mimetic menthol for the treatment of obesity. Upon subcutaneous injection, the as-developed hydrogel absorbs body fluids and gradually swells, enlarging its mesh and releasing its loaded menthol-CD inclusion complexes (IC). The cold-mimetic menthol then disassociates from the released IC to transform white adipocytes into beige adipocytes that exhibit enhanced UCP1 expression, triggering fat consumption and increasing energy expenditure. Meanwhile, the swelled (stretched) hydrogel networks drag the grafted liposomal nanocontrollers,

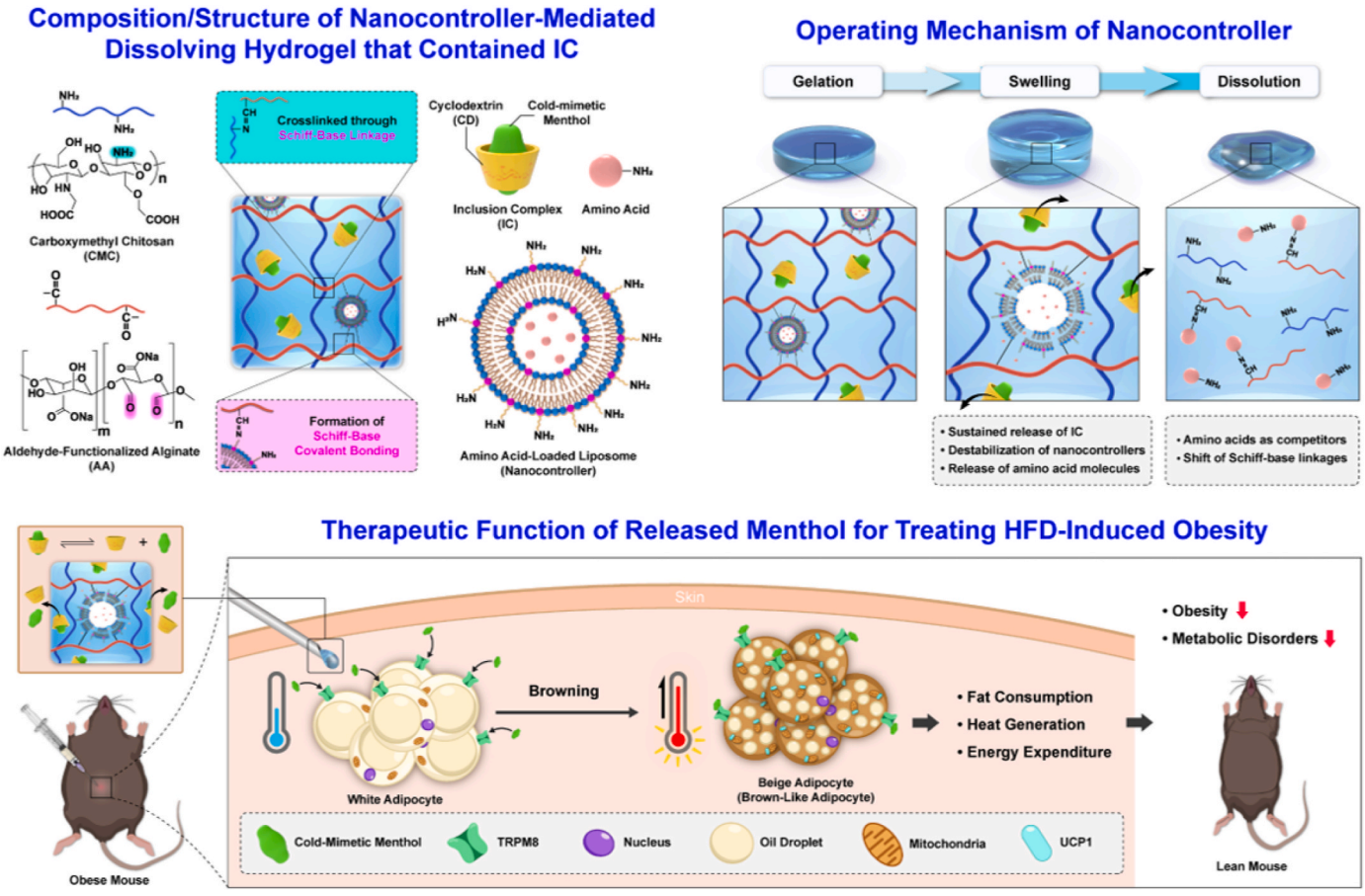

Fig. 1. Composition/structure of nanocontroller-mediated dissolving hydrogel that contained IC (IC@cLip-Gel), operating mechanism of nanocontroller, and adipocyte browning by released menthol for combating obesity and its related metabolic disorders in high-fat diet (HFD)-induced obese mice.

destabilize their lipid membrane, and thus cause the release of their loaded amino acid molecules. The released amino acid (glycine) molecules subsequently compete with the amines on CMC to react with aldehyde groups on AA, switching the dynamic Schiff-base linkages, ultimately causing hydrogel to dissolve. The thus-developed nanocontroller-mediated dissolving hydrogel realizes the sustained release of menthol for treating obesity, lowering body weight, improving obesity-related metabolic disorders, reducing the likelihood of type 2 diabetes and nonalcoholic fatty liver disease. Moreover, the built-in amino acid-loaded liposomal nanocontrollers make the hydrogel soluble after its payload is released, preventing the accumulation of hydrogel materials inside the body and consequent undesired adverse effects.

2. Materials and methods

2.1. Materials

Sodium alginate, sodium periodate ($NaIO_4$), menthol, hydroxypropyl-β-cyclodextrin (HP-β-CD), glycine, and choleserol were acquired from Sigma-Aldrich (St. Louis, MO, USA). CMC was purchased from Santa Cruz Biotechnology (Dallas, TX, USA). 1,2-dipalmitoyl-*sn*-glycero-3-phosphoethanolamine (DPPE) and 1,2-dipalmitoyl-*sn*-glycero-3-phosphocholine (DPPC) were procured from Avanti Polar Lipids (Alabaster, AL, USA). The murine preadipocyte cell line (3T3-L1) was obtained from the Bioresource Collection and Research Center of the Food Industry Research and Development Institute (Hsinchu, Taiwan). All other chemicals and reagents were analytical grade.

2.2. Synthesis and characterization of AA

AA was synthesized by a method that has been previously described [25]. In brief, sodium alginate (5 g) was dissolved in ethanol (20%). $NaIO_4$ (5.7 g) was then added to the as-prepared alginate solution, stirred for 7 h at room temperature in the dark. The reaction mixture was then terminated by adding ethylene glycol (10 mL) and sodium chloride (5 g). A mixture was precipitated out by adding cold absolute ethanol, and the precipitate was collected by filtration, before being dissolved in deionized (DI) water and purified by dialysis against DI water for three days. It was then lyophilized to obtain the AA. The as-obtained AA was characterized using Fourier-transform infrared (FT–IR) spectrometry (Nicolet iS50 spectrometer, Thermo Fisher Scientific, Waltham, MA, USA) and proton nuclear magnetic resonance (^{1}H NMR) spectrometry (Bruker AVANCE 600 MHz NMR spectrometer, Bruker BioSpin, Billerica, MA, USA).

2.3. Preparation and characterization of nanocontrollers (cLip)

Nanocontrollers (amino acid-loaded liposomes, cLip) were prepared using a thin-film hydration procedure with some minor modifications [26]. Briefly, DPPE and DPPC in a molar ratio of 1:4 were mixed in chloroform in a round-bottom flask. Upon removal of chloroform using a rotary evaporator (N-1200 A, EYELA, Tokyo, Japan), a lipid film formed in the round-bottom flask. This was then hydrated with aqueous glycine (1500 mM) under sonication to yield the glycine-loaded liposomal particles. These were extruded through a polycarbonate filter with a pore size of 100 nm using a mini-extruder (Avanti Polar Lipid) to obtain the cLip. Free glycine was removed by dialysis against DI water for three days.

The size and zeta potential of the obtained cLip were determined by dynamic light scattering (DLS, Litesizer 500, Anton Paar, Graz, Austria). The efficiency of loading glycine in the as-prepared cLip was measured using a glycine assay kit (MET-5070, Cell Biolabs, San Diego, CA, USA), and the physical stability of the cLip was evaluated by monitoring changes in their particle size and the amount of glycine that leaked into the solution over time.

2.4. Preparation and characterization of CMC-AA hydrogel (Gel)

The CMC-AA hydrogel (Gel) that was crosslinked through dynamic Schiff-base linkages was prepared from AA (2.5% by mass) and CMC (4%) at room temperature. The nanocontroller-mediated dissolving hydrogel was prepared by adding cLip (0.5%) into the Gel (cLip-Gel). The formed Schiff-base linkages between AA and CMC in the hydrogel were detected using high-resolution X-ray photoelectron spectrometry (XPS, ESCALAB 250, Thermo Fisher Scientific). The mechanical properties of the as-prepared hydrogel were determined using a rheometer (HR-2, TA Instruments, New Castle, DE, USA). Strain sweep measurements were made using a strain range from 1% to 1000% at a constant frequency of 1 Hz, and cyclic step-strain measurements were made at two strains (600% and 1%) at a frequency of 1 Hz [27].

To investigate the swelling and dissolution behaviors of the as-prepared hydrogels, test samples (200 μL) that were weighed immediately after gelation were incubated in a phosphate-buffered saline (PBS, 2 mL, pH 7.4) at 37 °C. Then, the incubated hydrogels were weighed after pre-determined durations (1 h, 6 h, 24 h, 48 h, 72 h, 96 h, 120 h, or 144 h). The swelling ratio was calculated as follows.

$$\text{Swelling Ratio}\ (\%) = \frac{W_{PBS} - W_i}{W_i} \times 100\%$$

where W_i is the initial weight of the hydrogel and W_{PBS} is the weight of the hydrogel after incubation in PBS for a particular time. The dissolution of a hydrogel in a body fluid reduces its remaining mass [28]. To determine its dissolution behavior, the test hydrogel was lyophilized and weighed after incubation in PBS for a particular time.

2.5. Preparation and characterization of IC

The menthol/HP-β-CD inclusion complex (IC) was prepared by a previously described procedure [20]. Briefly, menthol and HP-β-CD in a molar ratio of 1:1 were placed in DI water, stirred for 4 h at 40 °C, and then lyophilized to obtain the as-prepared IC, which was further analyzed using FT–IR spectroscopy and thermogravimetry (TGA, Mettler-Toledo, Columbus, OH, USA).

The loading content of menthol in the IC was determined using a colorimetric method that has been reported elsewhere [29]. Briefly, the as-prepared IC was dissolved in DI water (4.2 mg/mL, 50 μL), which was then mixed with methanol (50 μL) and a sulfuric acid solution (sulfuric acid:DI water = 1.6:1, by volume, 500 μL) that contained *p*-dimethyl amino benzaldehyde (DMAB, 0.5% by mass). The mixture was reacted in boiling water for 2 min. After cooling, the absorbance value of the mixture was measured at a wavelength of 550 nm using a spectrophotometer (Synergy HTX, BioTek, Santa Clara, CA, USA).

2.6. Release profile of menthol

The cumulative release profiles of menthol that were released from the test hydrogels in PBS at 37 °C for pre-determined durations were determined using the aforementioned colorimetric DMAB method.

2.7. Cytotoxicities of IC and test hydrogel

The cytotoxicity of IC was assessed by incubating it with 3T3-L1 cells, a murine preadipocyte cell line, in 96-well plates (5×10^4 cells per well). Twenty-four hours later, the cells were incubated with specific concentrations of IC (0, 25, 50, 100, and 250 μM, equivalent to the concentrations of the encapsulated menthol) for another 48 h. Cell viability was determined using a CCK-8 assay kit (Dojindo, Kumamoto, Japan). The cytotoxicity of the test hydrogel was evaluated using an elution test method [30]. In this investigation, the test hydrogel was incubated in Dulbecco's Modified Eagle's medium (DMEM, Corning, Glendale, AZ, USA) that contained 10% bovine calf serum (BCS, Sigma)

at 37 °C for 48 h to obtain the hydrogel extract, which was then co-cultured with 3T3-L1 cells for another 48 h so that the cell toxicity could be quantified.

2.8. Preparation of white adipocytes

To obtain white adipocytes, 3T3-L1 cells were subjected to a differentiation process [31]. Briefly, 3T3-L1 cells were grown in an expansion medium (DMEM with 10% BCS) for two days (approximately 100% confluence), incubated in a differentiation medium [DMEM with fetal bovine serum (FBS, 10%, Corning), 3-isobutyl-1-methylxanthine (0.5 mM), dexamethasone (1 μM), and insulin (10 μg/mL)] for two days, and then exposed to a maintenance medium [DMEM with FBS (10%) and insulin (10 μg/mL)] for another nine days. Following differentiation, cells were fixed with formaldehyde (4%) for 30 min at room temperature, stained with Oil Red O (ORO, 0.3% by volume) for 30 min, and observed under an optical microscope (Axio Observer 7, Carl Zeiss, Jena, Germany). Cell differentiation was verified by observing the accumulation of ORO-stained oil droplets inside the cells, which is a significant feature of white adipocytes [31].

2.9. Adipocyte browning induced by IC@cLip-Gel

The potential of the nanocontroller-mediated dissolving hydrogel that contained IC (IC@cLip-Gel) to induce the browning of white adipocytes was evaluated *in vitro*. The hallmark feature of adipocyte browning is the formation of beige adipocytes that express thermogenic UCP1, accompanied by the reductions in the amounts of contained oil droplets and triglycerides [32]. Therefore, the intracellular levels of UCP1, oil droplets, and triglycerides can be used to determine the degree of browning [32].

White adipocytes that had been treated with (IC@cLip-Gel) for 48 h were immunofluorescently stained with *anti*-UCP1 antibody (ab234430, Abcam, Cambridge, MA, USA) and then stained with secondary antibody (Alexa Flour 488-conjugated goat anti-rabbit IgG, abcam). The level of intracellularly expressed UCP1 was observed using a confocal laser scanning microscope (LSM 780; Carl Zeiss) and that of triglycerides was determined using a commercially available assay kit (ab65336, Abcam). To quantify the intracellular level of oil droplets, cells were stained with ORO and then eluted in absolute isopropanol; the absorbance of the obtained eluate was determined at a wavelength of 520 nm using a spectrophotometer (Synergy HTX, BioTek).

2.10. Animal study

Six-week-old male C57BL/6 J mice (National Laboratory Animal Center, Taipei, Taiwan) were used in an animal study. Animal experiments were carried out in a manner consistent with the "Guide for the Care and Use of Laboratory Animals" that was provided by the Institute of Laboratory Animal Resources, National Research Council, and published by the National Academy Press in 2011. The Institutional Animal Care and Use Committee of Academia Sinica approved the animal study protocols. To establish an obese animal model, mice were fed a high-fat diet (HFD, 60% of calories from fat, 58Y1, TestDiet, St. Louis, MO, USA) for nine weeks. Mice that had been fed a normal diet (13.5% of calories from fat, 5001, LabDiet, St. Louis, MO, USA) served as healthy controls.

2.11. In vivo therapeutic efficacy

The therapeutic efficacy of IC@cLip-Gel in cases of obesity was investigated in HFD-fed mice. Test mice were randomly divided into four groups; each was subcutaneously injected into the inguinal areas with PBS (100–150 μL, depending on animal body weight, as an untreated control), free IC (100–150 μL, containing 30 wt% of IC equivalent to menthol at 60 mg/kg), cLip-Gel (100–150 μL), or IC@cLip-Gel (100–150 μL, containing 30 wt% of IC equivalent to menthol at 60 mg/kg), twice weekly for two weeks.

During the period of treatment, animals continued to be fed with HFD; the body weight and food intake of each mouse were monitored. At the end of the experiment, the body composition of test mice was analyzed using time-domain (TD)-NMR (Minispec LF50, Bruker). Subsequently, the animals were sacrificed, and their subcutaneous WAT (sWAT) and epididymal WAT (eWAT) were harvested, weighed, and photographed to observe grossly their extent of fat accumulation. The harvested WAT was then divided into two parts; one part was homogenized to analyze pro-inflammatory cytokines and for UCP1 immunoblotting, while the other was fixed in formaldehyde (4%), embedded in paraffin, and sectioned for the histological (H&E) or immunohistochemical staining of UCP1.

For the pro-inflammatory cytokine and UCP1 immunoblotting analyses, WAT was lysed by RIPA lysis buffer (Merck-Millipore, Rahway, NJ, USA) with protease inhibitor cocktail (Merck-Millipore) using the gentleMACS Dissociator (Miltenyi Biotec, North Rhine-Westphalia, Germany). The levels of pro-inflammatory cytokines (IL-1β, TNFα, and IFNγ) in the homogenized tissues were measured by a multiplex assay (Bio-Plex Pro, Bio-Rad Laboratories, Hercules, USA). The expression of UCP1 in the homogenates was analyzed by immunoblotting. Briefly, proteins in the homogenates were separated on Bis-Tris gel electrophoresis (4–12%, SMOBIO, Hsinchu, Taiwan), and transferred to a polyvinylidene difluoride (PVDF) membrane (Bio-Rad Laboratories), which was then blocked with bovine serum albumin (2.5%) at room temperature for 1 h. The membrane was stained with *anti*-UCP1 antibody (ab234430, Abcam) at 4 °C overnight and then with secondary antibody (HRP-conjugated anti-rabbit IgG, Biolegend, San Diego, CA, USA). The expression of UCP1 was visualized by enhanced chemiluminescence substrates (Bio-Rad Laboratories) using a biospectrum imaging system (UVP, Upland, CA, USA).

2.12. Determination of levels of metabolic parameters

At the end of treatment, mice were challenged in an intraperitoneal glucose tolerance test (IPGTT). Briefly, the animals were fasted overnight (16 h) and then intraperitoneally injected with a glucose solution (2 g/kg body weight). Blood glucose levels were measured at predetermined time points using a glucose meter (Accu-Chek Instant S, Roche, Basel, Switzerland). The serum levels of cholesterol, triglycerides, aspartate transaminase (AST), and alanine transaminase (ALT) were measured using a chemistry analyzer (Dri-Chem 4000i, Fujifilm, Tokyo, Japan), and serum concentrations of insulin and leptin were determined using an insulin ELISA assay kit (10-1249-01, Mercodia, Uppsala, Sweden) and a leptin ELISA assay kit (10007609, Cayman, Ann Arbor, Michigan, USA), respectively.

2.13. Energy expenditure and body surface temperature

To study the influence of IC@cLip-Gel on the metabolic rate of test mice, their whole body energy metabolism was measured using a CLAMS-home cage system (Columbus Instruments, Columbus, OH, USA). The body surface temperature of each test mouse was monitored when it was fully awake, using an infrared thermal imaging camera (F30S, NEC Avio Infrared Technologies, Tokyo, Japan).

2.14. Statistical analysis

All results are presented as mean ± standard error. The unpaired Student *t*-test was used to compare data from two groups while one-way ANOVA followed by Tukey's post hoc test was used to identify differences among three or more groups. A P value of less than 0.05 was regarded as statistically significant.

3. Results and discussion

3.1. Characteristics of AA and CMC-AA hydrogel (Gel)

The C2 and C3 hydroxyl groups on sodium alginate were oxidized by $NaIO_4$ to form aldehyde-functionalized alginate (AA, Fig. 1). As shown in the FT–IR spectra (Fig. 2a), a new characteristic peak at 1730 cm^{-1}, indicative of the formation of aldehyde groups (–CHO) [33], was detected from the obtained AA. However, this characteristic peak of aldehyde groups was very weak owing to the immediate reaction of these groups with their adjacent hydroxyl groups to form hemiacetal bonds [33], as evidenced by the proton signal peaks at 5.3 and 5.6 ppm that were newly observed in the ^1H NMR spectrum of AA (Fig. 2b). These results demonstrate that alginate was successfully functionalized with aldehyde groups after being oxidized by $NaIO_4$.

The as-prepared AA then reacted with CMC to yield the CMC-AA hydrogel (Gel). The gelation time of the yielded Gel was around 21.5 min, as determined in a vial inversion test [30]. In the N 1s XPS spectrum of the Gel, a new binding energy peak at 398.6 eV, which could be assigned to the Schiff-base bonds (–C═N–), was detected (Fig. 2c) [34]. This finding reveals that the Gel was formed through Schiff-based linkages between the amines of CMC and the aldehyde groups of AA. The formation of Schiff-based linkages is known to be dynamically reversible [23].

To examine the injectability of the Gel, its rheological behaviors, including shear-thinning and self-healing properties, were examined

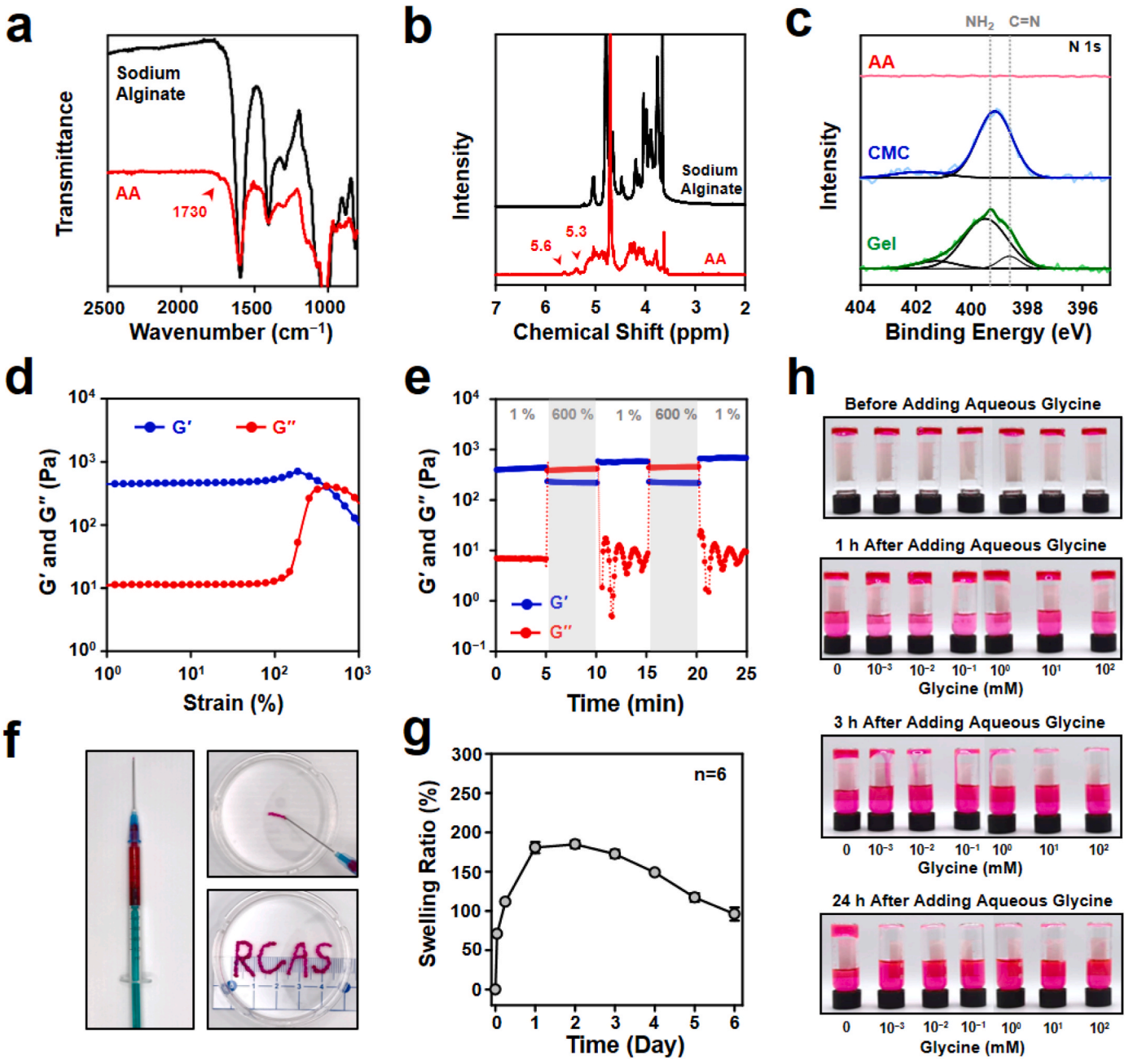

Fig. 2. Characteristics of AA and CMC-AA hydrogel (Gel). (a) FT–IR spectra and (b) ^1H NMR spectra of sodium alginate and AA. (c) N 1s XPS spectra of AA, CMC, and Gel. (d) Results of strain sweep test and (e) cyclic step-strain measurements of Gel. (f) Photographs showing injectability of Gel. (g) Swelling ratio of Gel when immersed in PBS at 37 °C for pre-determined durations. (h) Photographs of dissolution of Gel in aqueous glycine at various concentrations at 37 °C for pre-determined durations.

using a rheometer. The results that were obtained in a strain sweep test showed that the storage modulus (G′) of the Gel intersected the loss modulus (G″) at a strain of ~400%, which is its breaking strain [27] (Fig. 2d). Hence, the cyclic step-strain measurement of the Gel was conducted at a high strain of 600% (above the breaking strain) and a low strain of 1% (below the breaking strain) [27]. As indicated in Fig. 2e, following the mechanical disruption of the hydrogel by the high strain of 600%, its G″ was found to exceed its G′, showing that the test hydrogel underwent shear-thinning. Conversely, at the low strain of 1%, the G′ and G″ of the test hydrogel were promptly reverted to their initial values, demonstrating self-healing [27]. The shear-thinning and self-healing of the as-prepared Gel were probably caused by their dynamically reversible Schiff-base linkages, which rendered the as-formed hydrogel injectable [16,23]. The injectability of the Gel was further demonstrated by injecting it through a 23G needle, as shown in Fig. 2f.

To study the swelling capacity of the Gel, its swelling behavior was studied when it was immersed in PBS at 37 °C. As shown in Fig. 2g, the swelling ratio rapidly increased at first and then reached a maximum in around two days, indicating that the as-prepared Gel absorbed water, causing it to swell. During swelling, stretching of its network caused a conformational change [35].

Due to their dynamic reversibility, the coupling and uncoupling of the Schiff-base linkages in the network of the Gel occurred rapidly. Therefore, adding an amino acid might have disrupted the equilibrium of the Schiff-base linkages in the hydrogel, ultimately inducing its dissolution [24]. The amino acid-induced dissolution of the Gel was confirmed by adding an aqueous solution of the simplest amino acid, glycine, at distinct concentrations at 37 °C for pre-determined durations. To observe its dissolution clearly, a hydrophilic dye (rhodamine B, RhB) was mixed with the test hydrogel. As shown in Fig. 2h and S1, as the concentration of glycine increased, the dissolution of the hydrogel increased. At 24 h after incubation, the Gel had completely dissolved. These results reveal that the adding aqueous glycine induced the dissolution of the Gel.

3.2. Characteristics of nanocontroller-mediated dissolving hydrogel

To render the Gel soluble, glycine was loaded into liposomes whose surfaces contained amines, which could form covalent Schiff-base linkages (cLip, serving as nanocontrollers) with the aldehyde groups on AA that were present in the hydrogel network (cLip-Gel). The liposomal nanocontrollers were prepared from a lipid mixture of DPPE (which has a primary amine on its head group) and DPPC through a thin-film hydration procedure [26]. The loading efficiency of glycine in the liposomal nanocontrollers was around 35%. The as-prepared cLip had a size of 208.2 ± 19.6 nm and a zeta potential of −7.8 ± 0.5 mV, as determined by DLS (n = 6 batches). The physical stability of the cLip in aqueous solution was assessed by monitoring changes in their particle size and the amount of glycine that leaked into the solution over time. As shown in Fig. S2, no appreciable change in particle size or glycine leakage from the cLip was observed in three weeks, indicative of their stability.

During swelling, the hydrogel network of cLip-Gel was stretched, possibly dragging the cLip that were covalently grafted on the network, destabilizing their liposomal membranes and releasing their payload (glycine), ultimately causing the dissolution of the hydrogel. To study the mechanism of dissolution of cLip-Gel, the Gel in which was incorporated with free Lip (fLip-Gel) and that was covalently conjugated with empty Lip (eLip-Gel) were used as controls. The fLip was a glycine-loaded liposome whose surfaces did not contain amines, owing to the replacement of DPPE with cholesterol, preventing conjugation to the hydrogel network. Conversely, the eLip did not encapsulate glycine in its aqueous core but it had amine-containing surfaces, which could form covalent Schiff-base bonds with the aldehyde groups on AA inside the hydrogel network. As demonstrated by the N 1s XPS spectra, the Lip with amines on their surfaces (cLip and eLip) formed Schiff-base bonds with the aldehyde groups whereas fLip did not (Fig. 3a).

To evaluate the solubility of test hydrogels (fLip-Gel, eLip-Gel, and cLip-Gel), their swelling and dissolution behaviors in PBS at 37 °C were evaluated and compared. As shown in Fig. 3b, all test hydrogels swiftly absorbed water and rapidly swelled for the first 6 h. Thereafter, the two control hydrogels (fLip-Gel and eLip-Gel) continued to swell up to day 2, and their swelling behaviors were comparable to that of the Gel (Fig. 2g). In contrast, the swelling ratio of the cLip-Gel gradually declined after 6 h.

Following swelling, the dissolution of a hydrogel in a body fluid diminishes its remaining mass [28]. As indicated in Fig. 3c, the weight loss of cLip-Gel exceeded those of the control hydrogels ($P < 0.05$). This result was obtained because fLip released very little of their encapsulated glycine, whereas eLip did not contain glycine, so fLip-Gel and eLip-Gel lacked the capacity in dissolution. In contrast, the cLip-Gel that had built-in liposomal nanocontrollers (cLip) that could release glycine when triggered by swelling, was able to dissolve.

3.3. Characteristics of inclusion complexes (IC) and IC@cLip-Gel

The as-prepared cLip-Gel was loaded with cold-mimetic menthol to induce adipocyte browning. Menthol is lipophilic, making it difficult to load into the hydrophilic cLip-Gel. To improve its efficiency of loading in cLip-Gel, menthol was first included into HP-β-CD to form IC, which could then be readily incorporated into the hydrogel network [21].

The menthol-including IC was prepared in a menthol-to-HP-β-CD molar ratio of 1:1, following a procedure that has been described previously [20]. The as-prepared IC was characterized using FT–IR spectroscopy and TGA. In FT−IR spectra (Fig. 3d), characteristic peaks of the IC appeared at 3340, 2925, 1362, and 1032 cm^{-1}, and these were comparable to those of HP-β-CD. The characteristic peaks of menthol were absent from the spectrum of IC, implying that menthol was effectively included into the interior cavity of HP-β-CD [29]. Furthermore, as indicated in the TGA thermograms (Fig. 3e), most of the weight of pure menthol and HP-β-CD was lost at 50–130 °C and 300 °C, respectively [20]. In addition to exhibiting major weight loss at 300 °C, the as-prepared IC exhibited early weight loss at 180–300 °C owing to the evaporation of its included menthol. The results of the TGA also suggest the successful inclusion of menthol into HP-β-CD. The loaded content of menthol in the as-prepared IC was 62.9 ± 0.8 μg/mg (n = 6 batches), as determined using a colorimetric DMAB method [29].

The cytotoxicity of the as-prepared IC was then evaluated in 3T3-L1 cells. Fig. 3f demonstrates that cell viability was not influenced by the IC at various concentrations that corresponded to the specified concentrations of its entrapped menthol (25–250 μM, $P > 0.05$). Cold-mimetic menthol in a concentration range of 50–100 μM reportedly induces adipocyte browning *in vitro* [13,36], so the IC that contained 100 μM of menthol was selected in the subsequent studies.

Menthol that is loaded into the IC can be rapidly released in an aqueous environment [37], so maintaining a therapeutic concentration over an extended period is difficult. To overcome this difficulty, the as-prepared IC was loaded into the test hydrogels (IC@fLip-Gel, IC@eLip-Gel, and IC@cLip-Gel). Hydrogels are widely used for sustained release, as the steric interactions between the payload and the hydrogel network provide steric hindrance, which prevents rapid release [22].

To study whether hydrogels support the sustained release of menthol more than do free form IC (free IC), the release profiles of their menthol in PBS at 37 °C were studied. As presented in Fig. 3g, the menthol instantaneously dissociated from the free IC and reached a maximum concentration in the first hour. In contrast, the test hydrogels all exhibited the sustained release of menthol. Among the test hydrogels, IC@cLip-Gel released the most amount of menthol (~80%), probably because it had dissolved more quickly than IC@fLip-Gel and IC@eLip-Gel ($P < 0.05$, Fig. 3c). The dissolution behavior of hydrogel strongly

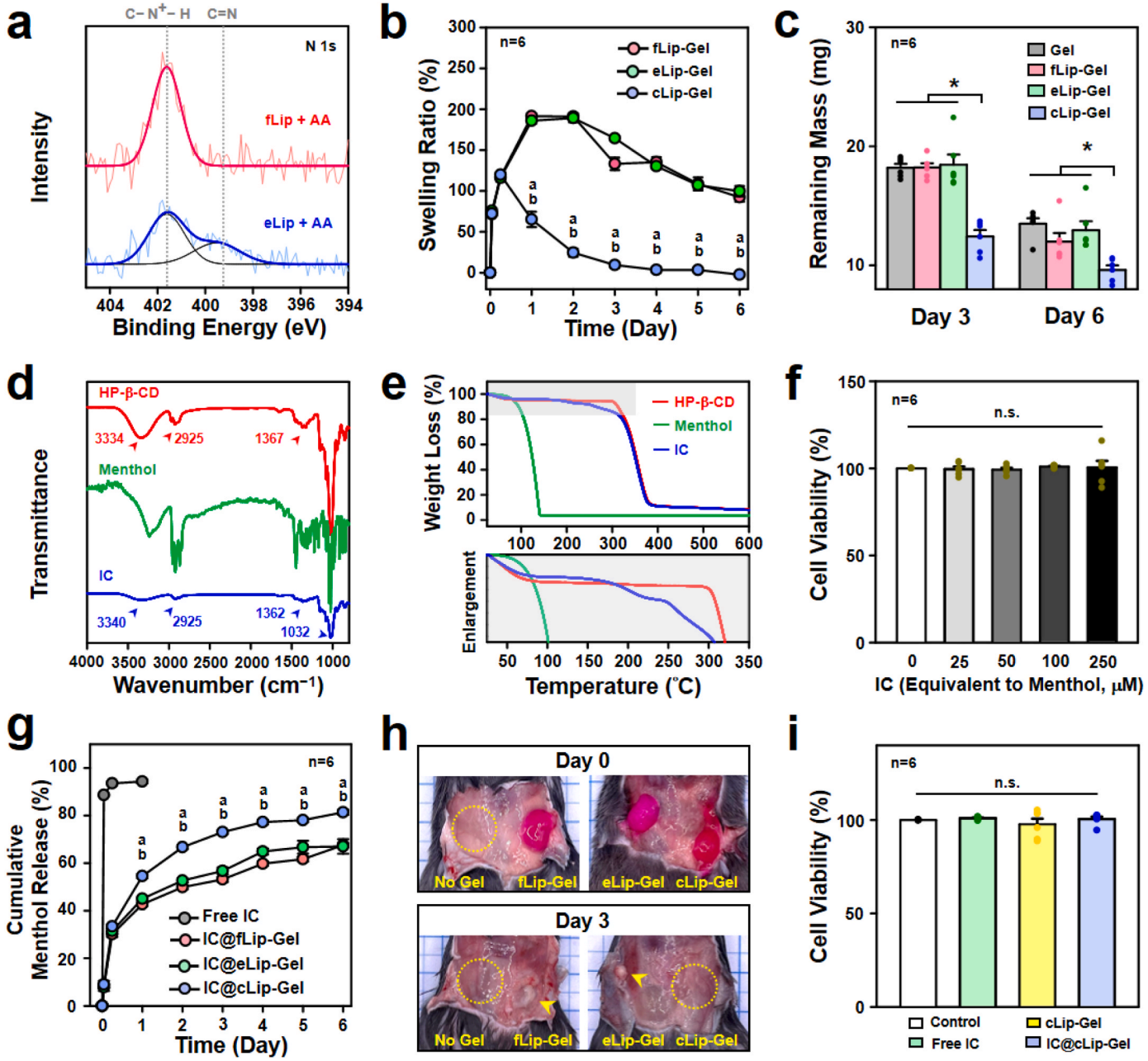

Fig. 3. Characteristics of cLip-Gel, IC and IC@cLip-Gel. (a) N 1s XPS spectra of fLip + AA and eLip + AA. (b) Swelling ratio and (c) remaining mass of test hydrogels when immersed in PBS at 37 °C for pre-determined durations. (d) FT–IR spectra and (e) TGA thermograms of HP-β-CD, menthol, and IC. (f) Cell viabilities of 3T3-L1 cells incubated with IC at various concentrations that corresponded to concentrations of encapsulated menthol. (g) Cumulative release profiles of menthol from free IC and various test hydrogels in PBS at 37 °C. (h) Photographs showing dissolution of test hydrogels in subcutaneous regions of test mice. For ease of observation, RhB was incorporated into the test hydrogels. (i) Cell viabilities of 3T3-L1 cells incubated with free IC, cLip-Gel, or IC@cLip-Gel. *: statistically significant ($P < 0.05$); [a]: $P < 0.05$ vs. fLip-Gel; [b]: $P < 0.05$ vs. eLip-Gel; n. s.: not significant ($P > 0.05$).

affects its release of a payload [22].

In vivo environments are always more complicated than *in vitro* environments [38]. The dissolution of as-prepared hydrogels was thus evaluated in subcutaneous regions in test mice. Three days following the subcutaneous injection of test hydrogels, fLip-Gel and eLip-Gel had left exogenous hydrogel materials at the injection site (Fig. 3h, indicated by yellow arrowheads), potentially causing undesired adverse effects. Conversely, cLip-Gel was absent because it had completely dissolved. This *in vivo* finding proves again that the dissolution rate of cLip-Gel exceeded those of fLip-Gel and eLip-Gel. Accordingly, only cLip-Gel was used in the following cell and animal studies.

The cytotoxicities of IC@cLip-Gel and its constituents (free IC and cLip-Gel) were examined using 3T3-L1 cells to ensure the safety of the sustained release system. None affected cell viability, as determined by comparison with an untreated control ($P > 0.05$, Fig. 3i), indicating that all components of IC@cLip-Gel were non-toxic.

3.4. *In vitro* adipocyte browning induced by IC@cLip-Gel

The induction of adipocyte browning holds great potential for treating obesity and its related metabolic disorders [7–9]. The potential of IC@cLip-Gel to induce adipocyte browning *in vitro* was assessed using white adipocytes, which were derived from 3T3-L1 cells (preadipocytes) that had undergone a differentiation process [31]; free IC and cLip-Gel

were used as controls. White adipocytes are characterized by their intracellular accumulation of oil droplets [31], which can be stained by ORO, a lipid-soluble dye [31]. As displayed in Fig. 4a, ORO-stained oil droplets were present inside 3T3-L1 cells that had been treated with differentiated media, confirming that the preadipocytes had successfully differentiated into white adipocytes.

Adipocyte browning is characterized by the emergence of beige adipocytes that express unique UCP1 proteins; this expression is accompanied by lipolysis, which is reflected by reductions in the amounts of intracellular oil droplets and triglycerides [32]. Accordingly, the levels of UCP1, oil droplets, and triglycerides that are expressed within adipocytes can be used to determine the extent of their browning [32]. As shown in Fig. 4b and c, as determined by comparison with untreated and cLip-Gel groups, a strong UCP1 fluorescence signal and a reduced area of ORO-stained oil droplets were detected in the white adipocytes that had been subjected to free IC or IC@cLip-Gel, revealing the formation of beige adipocytes. Additionally, the reductions in the levels of oil droplets (Fig. 4d) and triglycerides (Fig. 4e) in the white adipocytes in the free IC or IC@cLip-Gel groups exceeded those in the untreated and the cLip-Gel groups ($P < 0.05$). These results suggest that both free IC and IC@cLip-Gel induce adipocyte browning, triggering lipolysis (fat consumption), because they release cold-mimetic menthol.

3.5. *In vivo* therapeutic efficacy of IC@cLip-Gel

Since adipocyte browning can trigger fat consumption and increase energy expenditure [7–9], the therapeutic efficacies of IC@cLip-Gel against obesity and its related metabolic disorders were studied using an obese mouse model, which was fed with HFD for nine weeks. HFD-exposed mice gained much weight (*ca.* 37 g, Fig. S3a) after nine weeks of HFD intervention relative to normal diet-fed mice (*ca.* 27 g, $P < 0.05$). Fig. S3b shows that treatment with IC@cLip-Gel suppressed the weight gain of the test mice in a dose-dependent manner; the efficacy of IC@cLip-Gel was maximal at a dose of 60 mg cold-mimetic menthol per kg of body weight, which was thus selected for subsequent animal studies.

After nine-week HFD exposure, the test mice were divided into four groups; each was subcutaneously injected into inguinal areas with PBS, free IC, cLip-Gel, or IC@cLip-Gel, twice per week for two weeks (on days 0, 3, 7 and 10; Fig. S4). During the period of treatment, the body weight and food intake of each test mouse were monitored. The body weight (Fig. 5a) of the HFD mice that received IC@cLip-Gel was markedly lower

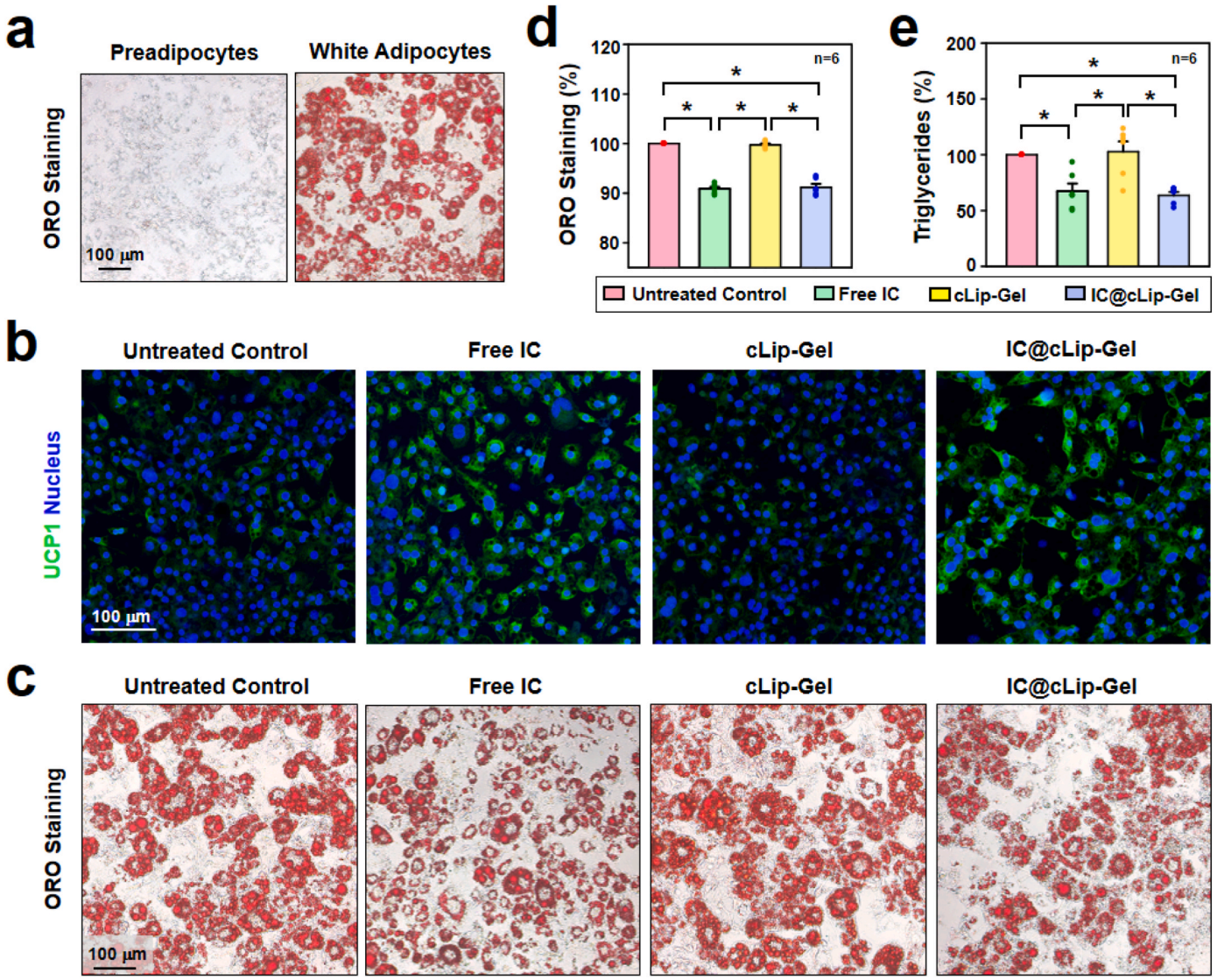

Fig. 4. Adipocyte browning *in vitro*. (a) Photographs of oil droplet accumulation in 3T3-L1 cells that had been treated with differentiated media. (b) CLSM images of cellular levels of UCP1 expression, (c) photographs of oil droplets, (d) corresponding quantitative analysis, and (e) cellular levels of triglycerides in white adipocytes following various treatments. *: statistically significant ($P < 0.05$).

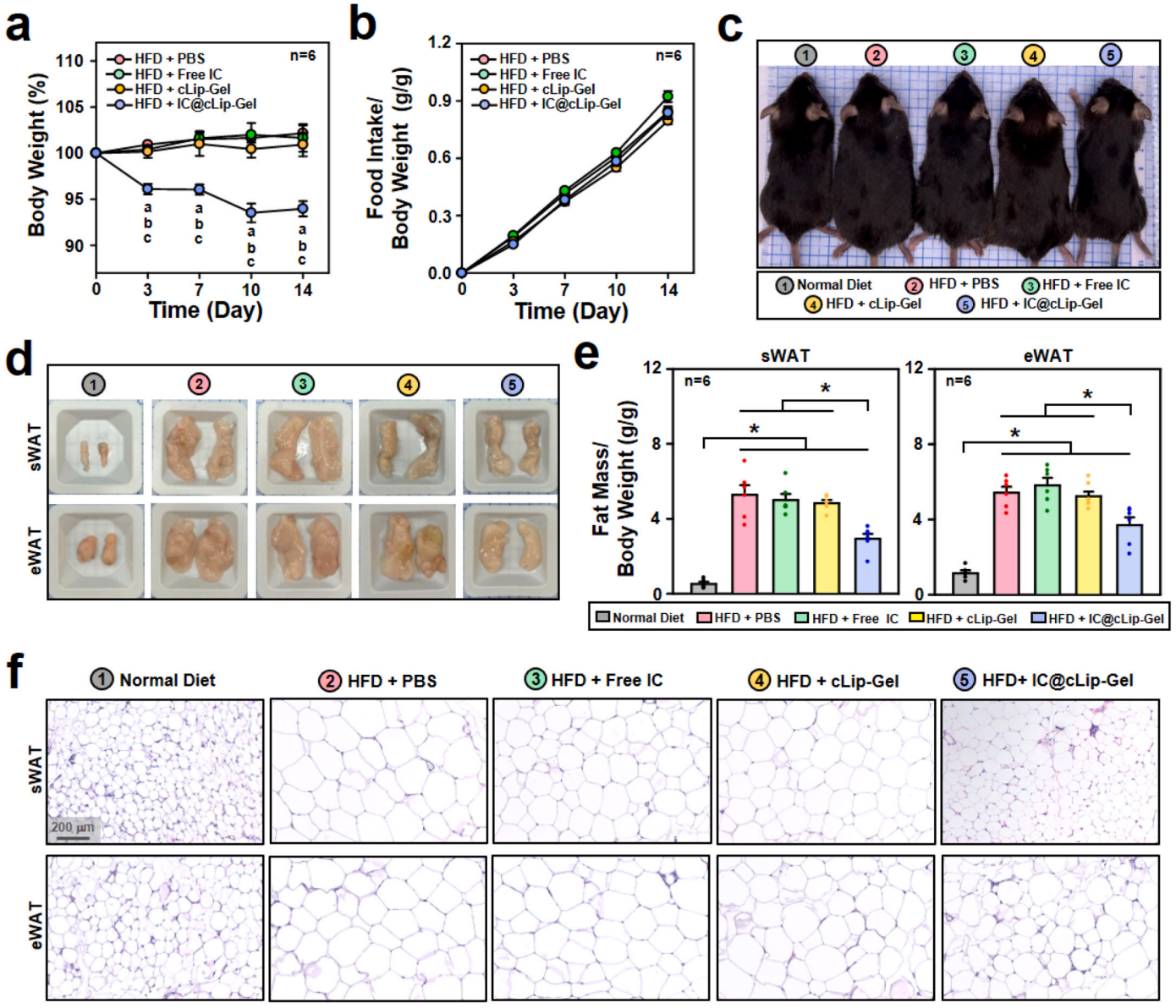

Fig. 5. Therapeutic efficacy of IC@cLip-Gel in HFD-induced obese mice. (a) Relative body weight changes and (b) food intake of test mice during various treatments. (c) Photographs of test mice at end of various treatments. (d) Photographs of sWAT and eWAT that were harvested from test mice at end of treatment and (e) their relative masses. (f) H&E staining images of sWAT and eWAT harvested from test mice that had received various treatments at end of experiment. *: statistically significant ($P < 0.05$); [a]: $P < 0.05$ vs. HFD + PBS; [b]: $P < 0.05$ vs. HFD + Free IC; [c]: $P < 0.05$ vs. HFD + cLip-Gel.

than that of the mice that received control treatments ($P < 0.05$) at each monitoring point (days 3, 7, 10, and 14), even though their food intakes did not differ ($P > 0.05$, Fig. 5b). At the end of the treatment, the HFD mice in the IC@cLip-Gel-treated group appeared to be smaller than those in the control groups (Fig. 5c). The changes in body weight and gross appearances were attributed to a loss of body white fat mass, including subcutaneous WAT (sWAT) and epididymal WAT (eWAT) (Fig. 5d and e). Additionally, treatment with IC@cLip-Gel caused a greater reduction in the sizes of white adipocytes in WAT than in the control counterparts (Fig. 5f), possibly owing to the intracellular consumption of oil droplets (Fig. 4c and d) and triglycerides (Fig. 4e). The obtained results reveal the anti-obesity effectiveness of the as-proposed IC@cLip-Gel.

In this study, administering IC@cLip-Gel subcutaneously into the inguinal areas of HFD mice reduced fat mass and sizes of white adipocytes not only in the administered region (sWAT) but also in the distant adipose tissues (eWAT), indicating the potential of IC@cLip-Gel for remote browning action. These findings are also consistent with previously published results [8,39].

The body composition (including lean mass and fat mass) of the HFD mice in the IC@cLip-Gel group was assessed using TD-NMR; the mice that were treated with PBS served as a control (untreated). The mice that received IC@cLip-Gel had a greater lean mass and a lower fat mass than the untreated mice ($P < 0.05$, Fig. S5).

In the current work, treatment with free IC twice weekly did not inhibit HFD-induced obesity (Fig. 5a, 5c–5f), probably because the release of menthol from the free IC was too rapid to maintain a therapeutic concentration. To manage the body weight, frequent administration of the therapeutic compound is therefore required, potentially leading to poor patient compliance. By contrast, IC@cLip-Gel released menthol sustainably (Fig. 3g), inducing adipocyte browning, causing the consumption of fat in WAT.

Studies have shown that HFD-induced obesity is a state of chronic inflammation in WAT, in which proinflammatory cytokines, including

IL-1β, TNFα, and IFNγ, are overproduced [40,41]. As confirmed in this study, the WAT that was collected from the mice that received HFD produced markedly more proinflammatory cytokines (IL-1β, TNFα, and IFNγ) than those that were harvested from the mice on a normal diet (Fig. 6a–c). Notably, the decline in the overproduced proinflammatory cytokines in the HFD mice upon treatment with IC@cLip-Gel exceeded that upon treatment with PBS, free IC, or cLip-Gel (with some statistically insignificant), demonstrating the potential of IC@cLip-Gel to alleviate obesity-induced inflammatory responses in WAT.

The HFD-induced overproduction of proinflammatory cytokines reportedly impairs the systemic metabolic function, causing metabolic disorders, such as hypercholesterolemia, hypertriglyceridemia, hyperinsulinemia, hyperleptinemia, and hyperglycosemia, ultimately increasing incidences of type 2 diabetes and nonalcoholic fatty liver diseases [5,42]. Whether treatment with IC@cLip-Gel can improve the metabolic function of HFD-induced obese mice was explored herein. At the end of the experiment, levels of serum cholesterol, triglycerides, insulin, leptin, and blood glucose in HFD mice that received IC@cLip-Gel were much lower than in those that received control treatments (Fig. 6d–h).

To evaluate their glucose metabolism, test mice were challenged by IPGTT [7,8]. The glucose tolerance of HFD mice was poorer than that of mice that had been fed on a normal diet (Fig. 6i). The treatment of HFD mice with IC@cLip-Gel significantly improved their glucose tolerance above that of controls (Fig. 6i). The obtained data support the claim that the HFD mice that were treated with IC@cLip-Gel showed improved systemic metabolic functions.

Excess caloric intake in HFD mice can cause fat accumulation not only in their WAT but also in liver tissues, resulting in hepatic dysfunctions, including the accumulation of oil droplets, a decrease in

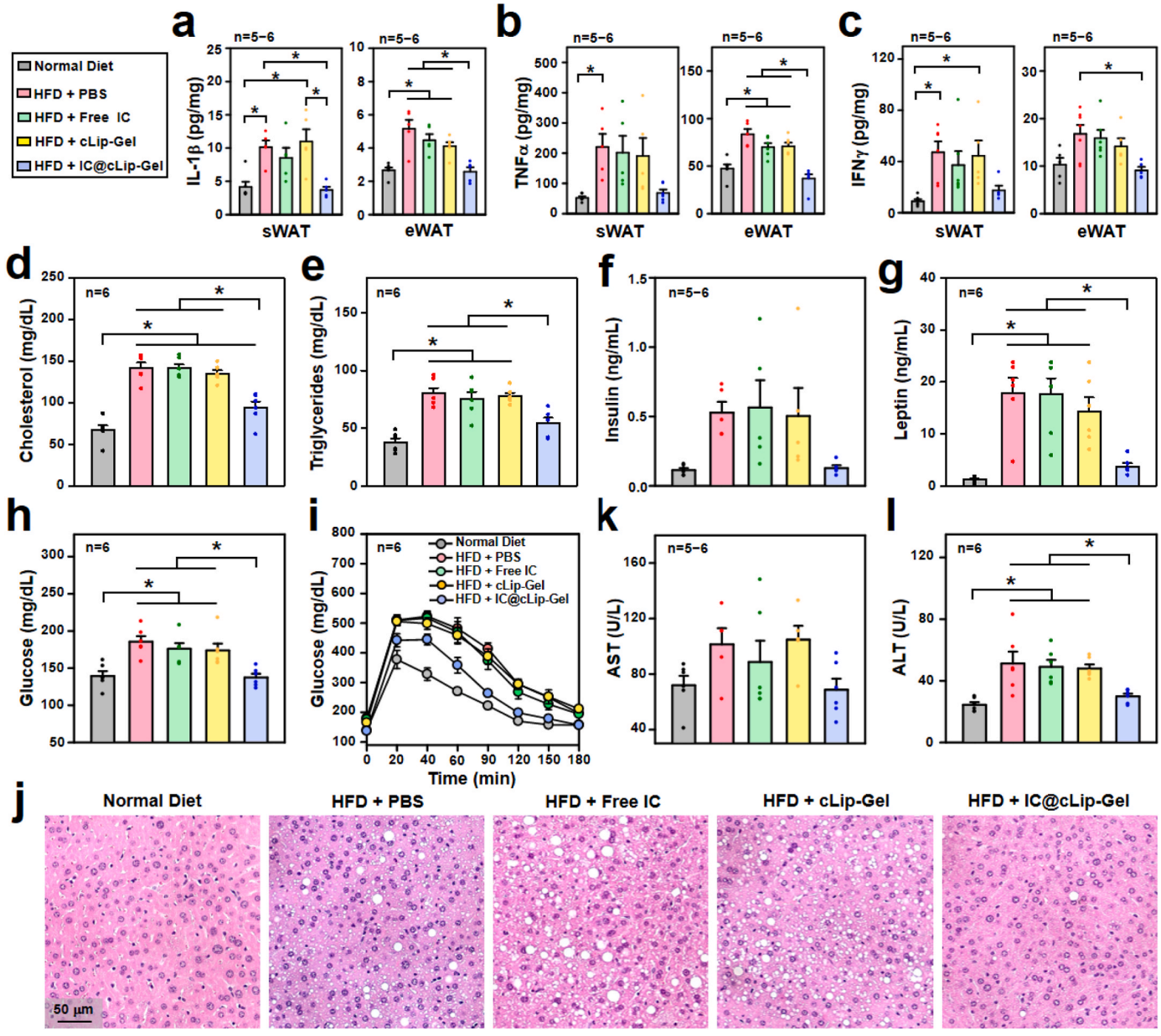

Fig. 6. Therapeutic effects of IC@cLip-Gel on obesity-induced chronic inflammation and metabolic disorders. Inflammatory cytokine levels of (a) IL-1β, (b) TNFα, and (c) IFNγ in sWAT and eWAT retrieved from test mice at end of treatment. Levels of (d) serum cholesterol, (e) serum triglycerides, (f) serum insulin, (g) serum leptin, and (h) blood glucose in test mice that had received various treatments at end of experiment. (i) Changes of blood glucose levels in test mice that were challenged by IPGTT. (j) H&E staining images of liver tissues, (k) serum AST levels, and (l) serum ALT levels collected from test mice that had received various treatments at end of experiment. *: statistically significant ($P < 0.05$).

glycogen deposition, and high serum levels of AST and ALT [43,44]. The accumulation of excess lipids reportedly disrupts the energy metabolism by utilizing glycogen as an energy source [44]. The group that received IC@cLip-Gel exhibited less fat accumulation (H&E staining, Fig. 6j) and increased glycogen deposition (PAS staining, Fig. S6) in liver tissues, as well as lower levels of serum AST and ALT (Fig. 6k and l) than did the control groups, proving that treatment with IC@cLip-Gel effectively protects mice against HFD-induced hepatic dysfunctions.

3.6. *WAT browning induced by IC@cLip-Gel*

WAT browning, which can trigger the consumption of fat and expenditure of energy, is characterized by the expression of thermogenic UCP1, which is indicative of the appearance of beige adipocytes in WAT [7]. The extent of WAT browning in the HFD mice that received IC@cLip-Gel was examined; the mice that received PBS, free IC, or cLip-Gel served as controls. Fig. 7a reveals that the level of UCP1 that was expressed in WAT, or the extent of WAT browning, was higher in the IC@cLip-Gel-treated group than in the control-treated groups; this finding is consistent with the results of the immunoblotting of UCP1 expressions (Fig. 7b). These results altogether suggest that in the mice that were treated with IC@cLip-Gel, white adipocytes in WAT were effectively transformed into thermogenic beige adipocytes, as reflected by their high body surface temperatures (Fig. 7c).

The induction of WAT browning is known to increase energy expenditure or metabolic rate [39,45]. To study the influence of IC@cLip-Gel on the metabolic rate of HFD mice, their whole-body energy metabolism was monitored following its subcutaneous injection. The IC@cLip-Gel-treated mice exhibited significantly higher rates of oxygen consumption (VO_2, $P < 0.05$, Fig. 7d), carbon dioxide generation (VCO_2, $P < 0.05$, Fig. 7e), and heat production ($P < 0.05$, Fig. 7f) than the PBS-treated mice in both light and dark periods. These data demonstrate that treatment with IC@cLip-Gel increased the energy expenditure of HFD mice, probably due to its ability to induce the browning of WAT.

Regaining body weight after withdrawal of weight loss treatments is undesirable. In this study, the changes of body weight in mice that were treated with IC@cLip-Gel did not show a significant difference between day 22 (12 days after the final treatment) and day 10 (Fig. S7, $P > 0.05$). However, there was a slight trend of weight regain observed, which could be attributed to the reversible nature of browning in white adipose tissue, where beige adipocytes gradually convert back to white adipocytes once the environmental stimuli are removed [46]. To sustain improvements in body weight and metabolic functions, ongoing use of browning agents may be required.

To assess the *in vivo* safety of IC@cLip-Gel, the major organs and the muscle and skin tissues that were in contact with the test hydrogel were collected from the HFD mice at the end of the experiments for histological examination. No obvious abnormality or inflammation was observed in any of the collected tissue sections (Fig. S8), indicating the biocompatibility of the as-designed IC@cLip-Gel.

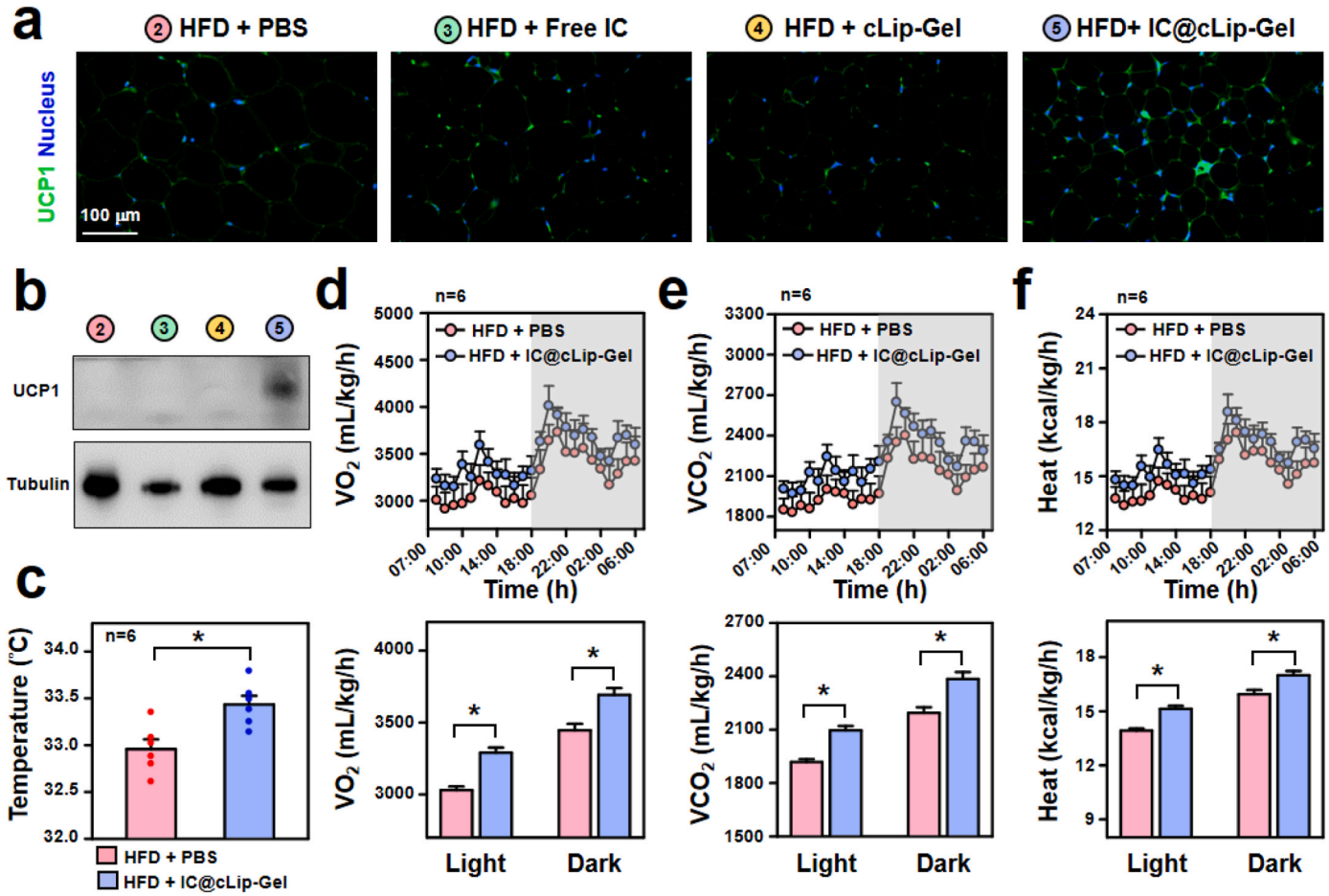

Fig. 7. Adipocyte browning *in vivo*. (a) Fluorescent images and (b) immunoblotting images of UCP1 expressed in sWAT obtained from test mice that had received various treatments at end of experiment. (c) Average surface temperature of inguinal area of test mice that had been treated with PBS or IC@cLip-Gel. (d) Oxygen consumption (VO_2), (e) carbon dioxide generation (VCO_2), and (f) heat production of test mice that had received PBS or IC@cLip-Gel at end of experiment.

4. Conclusions

This work develops a nanocontroller-mediated dissolving hydrogel that sustainably releases cold-mimetic menthol to induce adipocyte browning in the WAT of HFD-induced obese mice. Following subcutaneous injection, the as-developed hydrogel absorbs body fluids and swells, releasing its loaded IC. The menthol then disassociates from the released IC to transform the white adipocytes in WAT into thermogenic beige adipocytes, triggering fat consumption and heat generation, increasing energy expenditure, ultimately alleviating the HFD-induced obesity and its related metabolic disorders, which include hyperlipidemia, impaired glucose tolerance, and hepatic dysfunctions. Meanwhile, the swelled hydrogel networks destabilize the membranes of the grafted liposomal nanocontrollers, releasing their encapsulated glycine molecules, eventually causing the dissolution of the hydrogel *in situ*. Overall, the as-developed nanocontroller-mediated dissolving hydrogel not only favors the sustained release of therapeutic menthol for treating obesity and its related metabolic disorders but also prevents the adverse effects that are associated with the accumulation of the retention of hydrogels within the body.

Credit author statement

Ting Ruan: Conceptualization, Investigation, Funding acquisition, Visualization, Writing – original draft. **Chih-Yu Fu:** Investigation, Methodology, Formal analysis, Validation, Writing – original draft. **Chih-Hung Lin:** Conceptualization, Funding acquisition, Writing – original draft. **Kun-Chi Chou:** Investigation, Methodology. **Yu-Jung Lin:** Conceptualization, Investigation, Funding acquisition, Formal analysis, Supervision, Writing – original draft.

Declaration of competing interest

The authors declare that they have no known competing financial interests or personal relationships that could have appeared to influence the work reported in this paper.

Data availability

Data will be made available on request.

Acknowledgments

This work was supported by grant from the National Science and Technology Council (110-2222-E-001-001-MY3) of Taiwan and the grant from the Cathay General Hospital (111-CGH-FJU-09), Taipei, Taiwan. The authors thank the Taiwan Mouse Clinic, Academia Sinica and Taiwan Animal Consortium for the technical support in the examination of body surface temperature, whole body energy metabolism as well as body composition, and the Academia Sinica Inflammation Core Facility, IBMS for technical support in the determination of levels of proinflammtory cytokines. The core facility is funded by the Academia Sinica Core Facility and Innovative Instrument Project (AS-CFII-111-213).

Appendix A. Supplementary data

Supplementary data to this article can be found online at https://doi.org/10.1016/j.biomaterials.2023.122120.

References

[1] M. Blüher, Obesity: global epidemiology and pathogenesis, Nat. Rev. Endocrinol. 15 (2019) 288–298.
[2] J. Li, R. Cha, H. Luo, W. Hao, Y. Zhang, X. Jiang, Nanomaterials for the theranostics of obesity, Biomaterials 223 (2019), 119474.
[3] D.M. Williams, A. Nawaz, Marc Evans, Drug therapy in obesity: a review of current and emerging treatments, Diabetes Ther 11 (2020) 1199–1216.
[4] F. Stenard, A. Iannelli, Laparoscopic sleeve gastrectomy and gastroesophageal reflux, World J. Gastroenterol. 21 (2015) 10348–10357.
[5] C.M. Kusminski, P.E. Bickel, P.E. Scherer, Targeting adipose tissue in the treatment of obesity-associated diabetes, Nat. Rev. Drug Discov. 15 (2016) 639–660.
[6] L. Ye, J. Wu, P. Cohen, L. Kazak, M.J. Khandekar, M.P. Jedrychowski, X. Zeng, S. P. Gygi, B.M. Spiegelman, Fat cells directly sense temperature to activate thermogenesis, Proc. Natl. Acad. Sci. U. S. A. 110 (2013) 12480–12485.
[7] A. Than, P.K. Duong, P. Zan, J. Liu, M.K.S. Leow, P. Chen, Lancing drug reservoirs into subcutaneous fat to combat obesity and associated metabolic diseases, Small 16 (2020), 2002872.
[8] P. Zan, A. Than, W. Zhang, H.X. Cai, W. Zhao, P. Chen, Transdermal photothermal-pharmacotherapy to remodel adipose tissue for obesity and metabolic disorders, ACS Nano 16 (2022) 1813–1825.
[9] Y. Zu, L. Zhao, L. Hao, Y. Mechref, M. Zabet-Moghaddam, P.A. Keyel, M. Abbasi, D. Wu, J.A. Dawson, R. Zhang, S. Nie, N. Moustaid-Moussaa, M.G. Kolonin, A. C. Daquinag, L. Brandi, I. Warraich, S.K.S. Francisco, X. Sun, S. Wang, Browning white adipose tissue using adipose stromal cell-targeted resveratrol-loaded nanoparticles for combating obesity, J. Contr. Release 333 (2021) 339–351.
[10] Z.S. Clayton, C.E. McCurdy, Short-term thermoneutral housing alters glucose metabolism and markers of adipose tissue browning in response to a high-fat diet in lean mice, Am. J. Physiol. Regul. Integr. Comp. Physiol. 315 (2018) R627–R637.
[11] R.K. Srivastava, A. Moliner, E.S. Lee, E. Nickles, E. Sim, C. Liu, H. Schwarz, C. F. Ibáñez, CD137 negatively affects "browning" of white adipose tissue during cold exposure, J. Biol. Chem. 295 (2020) 2034–2042.
[12] C. Clemmensen, S. Jall, M. Kleinert, C. Quarta, T. Gruber, J. Reber, S. Sachs, K. Fischer, A. Feuchtinger, A. Karlas, S.E. Simonds, G. Grandl, D. Loher, E. Sanchez-Quant, S. Keipert, M. Jastroch, S.M. Hofmann, E.B.M. Nascimento, P. Schrauwen, V. Ntziachristos, M.A. Cowley, B. Finan, T.D. Müller, M.H. Tschöp, Coordinated targeting of cold and nicotinic receptors synergistically improves obesity and type 2 diabetes, Nat. Commun. 9 (2018) 4304.
[13] C. Jiang, M. Zhai, D. Yan, D. Li, C. Li, Y. Zhang, L. Xiao, D. Xiong, Q. Deng, W. Sun, Dietary menthol-induced TRPM8 activation enhances WAT "browning" and ameliorates diet-induced obesity, Oncotarget 8 (2017) 75114–75126.
[14] P. Khare, P. Mangal, R.K. Baboota, S. Jagtap, V. Kumar, D.P. Singh, R.K. Boparai, S. S. Sharma, R. Khardori, S.K. Bhadada, K.K. Kondepudi, K. Chopra, M. Bishnoi, Involvement of glucagon in preventive effect of menthol against high fat diet induced obesity in mice, Front. Pharmacol. 9 (2018) 1244.
[15] P. Khare, A. Chauhan, V. Kumar, J. Kaur, N. Mahajan, V. Kumar, A. Gesing, K. Chopra, K.K. Kondepudi, M. Bishnoi, Bioavailable menthol (transient receptor potential melastatin-8 agonist) induces energy expending phenotype in differentiating adipocytes, Cells 8 (2019) 383.
[16] X. Wu, C. He, Y. Wu, X. Chen, Synergistic therapeutic effects of Schiff's base cross-linked injectable hydrogels for local co-delivery of metformin and 5-fluorouracil in a mouse colon carcinoma model, Biomaterials 75 (2016) 148–162.
[17] K.Y. Lee, D.J. Mooney, Alginate: properties and biomedical applications, Prog. Polym. Sci. 37 (2012) 106–126.
[18] L. Upadhyaya, J. Singh, V. Agarwal, R.P. Tewari, Biomedical applications of carboxymethyl chitosans, Carbohydr. Polym. 91 (2013) 452–466.
[19] Z. Hu, S. Li, S. Wang, B. Zhang, Q. Huang, Encapsulation of menthol into cyclodextrin metal-organic frameworks: preparation, structure characterization and evaluation of complexing capacity, Food Chem. 338 (2021), 127839.
[20] Z.I. Yildiz, A. Celebioglu, M.E. Kilic, E. Durgun, T. Uyar, Menthol/cyclodextrin inclusion complex nanofibers: enhanced water-solubility and high-temperature stability of menthol, J. Food Eng. 224 (2018) 27–36.
[21] J. Wankar, N.G. Kotla, S. Gera, S. Rasala, A. Pandit, Y.A. Rochev, Recent advances in host–guest self-assembled cyclodextrin carriers: implications for responsive drug delivery and biomedical engineering, Adv. Funct. Mater. 30 (2020), 1909049.
[22] J. Li, D.J. Mooney, Designing hydrogels for controlled drug delivery, Nat. Rev. Mater. 1 (2016), 16071.
[23] M.R. Arkenberg, H.D. Nguyen, C.C. Lin, Recent advances in bio-orthogonal and dynamic crosslinking of biomimetic hydrogels, J. Mater. Chem. B 8 (2020) 7835–7855.
[24] W. Huang, Y. Wang, Z. Huang, X. Wang, L. Chen, Y. Zhang, L. Zhang, On-demand dissolvable self-healing hydrogel based on carboxymethyl chitosan and cellulose nanocrystal for deep partial thickness burn wound healing, ACS Appl. Mater. Interfaces 10 (2018) 41076–41088.
[25] Y. Xu, C. Huang, L. Li, X. Yu, X. Wang, H. Peng, Z. Gu, Y. Wang, In vitro enzymatic degradation of a biological tissue fixed by alginate dialdehyde, Carbohydr, Polymer 95 (2013) 148–154.
[26] W.L. Wan, B. Tian, Y.J. Lin, C. Korupalli, M.Y. Lu, Q. Cui, D. Wan, Y. Chang, H. W. Sung, Photosynthesis-inspired H_2 generation using a chlorophyll-loaded liposomal nanoplatform to detect and scavenge excess ROS, Nat. Commun. 11 (2020) 534.
[27] Y. Liu, S.H. Lin, W.T. Chuang, N.T. Dai, S.H. Hsu, Biomimetic strain-stiffening in chitosan self-healing hydrogels, ACS Appl. Mater. Interfaces 14 (2022) 16032–16046.
[28] S. Li, N. Chen, X. Li, Y. Li, Z. Xie, Z. Ma, J. Zhao, X. Hou, X. Yuan, Bioinspired double-dynamic-bond crosslinked bioadhesive enables post-wound closure care, Adv. Funct. Mater. 30 (2020), 2000130.
[29] X. Wu, P. Li, L. Cong, H. Yu, D. Zhang, Y. Yue, H. Xu, K. Xu, X. Zheng, X. Wang, Electrospun poly(vinyl alcohol) nanofiber films containing menthol/β-cyclodextrin inclusion complexes for smoke filtration and flavor retention, Colloids Surf. A Physicochem. Eng. Asp. 605 (2020), 12537.

[30] N. Nguyen, Z.H. Lin, S.R. Barman, C. Korupalli, J.Y. Cheng, N.X. Song, Y. Chang, F. L. Mi, H.L. Song, H.W. Sung, Y.J. Lin, Engineering an integrated electroactive dressing to accelerate wound healing and monitor noninvasively progress of healing, Nano Energy (2022), 107393.
[31] E.J. Jeon, D.Y. Kim, N.H. Lee, H.E. Choi, H.G. Cheon, Telmisartan induces browning of fully differentiated white adipocytes via M2 macrophage polarization, Sci. Rep. 9 (2019) 1236.
[32] M. Sudhakar, S.J. Sasikumar, S. Silambanan, D. Natarajan, R. Ramakrishnan, A. J. Nair, M.S. Kiran, Chlorogenic acid promotes development of brown adipocyte-like phenotype in 3T3-L1 adipocytes, J. Funct.Foods 74 (2020), 104161.
[33] L. Wang, Y. Hou, X. Zhong, J. Hu, F. Shi, H. Mi, Preparation and catalytic performance of alginate-based Schiff Base, Carbohydr. Polym. 208 (2019) 42–49.
[34] W.R. Cui, C.R. Zhang, W. Jiang, F.F. Li, R.P. Liang, J. Liu, J.D. Qiu, Regenerable and stable sp2 carbon-conjugated covalent organic frameworks for selective detection and extraction of uranium, Nat. Commun. 11 (2020) 436.
[35] F. Wu, Y. Pang, J. Liu, Swelling-strengthening hydrogels by embedding with deformable nanobarriers, Nat. Commun. 11 (2020) 4502.
[36] M. Rossato, M. Granzotto, V. Macchi, A. Porzionato, L. Petrelli, A. Calcagno, J. Vencato, D.D. Stefani, V. Silvestrin, R. Rizzuto, F. Bassetto, R.D. Carob, R. Vettor, Human white adipocytes express the cold receptor TRPM8 which activation induces UCP1 expression, mitochondrial activation and heat production, Mol. Cell. Endocrinol. 383 (2014) 137–146.
[37] V.J. Stella, V.M. Rao, E.A. Zannou, V. Zia, Mechanisms of drug release from cyclodextrin complexes, Adv. Drug Deliv. Rev. 36 (1999) 3–16.
[38] W.B. Mattes, In vitro to in vivo translation, Curr. Opin. Toxicol 23 (2020) 114–118.
[39] Y. Zhang, Q. Liu, J. Yu, S. Yu, J. Wang, L. Q, Z. Gu, Locally induced adipose tissue browning by microneedle patch for obesity treatment, ACS Nano 11 (2017) 9223–9230.
[40] E.A. Lima, L.S. Silveira, L.N. Masi, A.R. Crisma, M.R. Davanso, G.I.G. Souza, A. B. Santamarina, R.G. Moreira, A.R. Martins, L.G.O. de Sousa, S.M. Hirabara, J.C. R. Neto, Macadamia oil supplementation attenuates inflammation and adipocyte hypertrophy in obese mice, Mediat. Inflamm. 2014 (2014), 870634.
[41] Y. Wang, B. Tang, L. Long, P. Luo, W. Xiang, X. Li, H. Wang, Q. Jiang, X. Tan, S. Luo, H. Li, Z. Wang, Z. Chen, Y. Leng, Z. Jiang, Y. Wang, L. Ma, R. Wang, C. Zeng, Z. Liu, Y. Wang, H. Miao, C. Shi, Improvement of obesity-associated disorders by a small-molecule drug targeting mitochondria of adipose tissue macrophages, Nat. Commun. 12 (2021) 102.
[42] S.K. Wong, K.Y. Chin, F.H. Suhaimi, A. Fairus, S. Ima-Nirwana, Animal models of metabolic syndrome: a review, Nutr. Metab. 13 (2016) 65.
[43] E. Fabbrini, S. Sullivan, Samuel Klein, Obesity and nonalcoholic fatty liver disease: biochemical, metabolic, and clinical implications, Hepatology 51 (2010) 679–689.
[44] C.J. Liou, S.J. Wu, S.C. Shen, L.C. Chen, Y.L. Chen, W.C. Huang, Phloretin ameliorates hepatic steatosis through regulation of lipogenesis and Sirt1/AMPK signaling in obese mice, Cell Biosci. 10 (2020) 114.
[45] J. Qiu, Q. Fan, S. Xu, D. Wang, J. Chen, S. Wang, T. Hu, X. Ma, Y. Cheng, L. Xu, A fluorinated peptide with high serum-and lipid-tolerence for the delivery of siRNA drugs to treat obesity and metabolic dysfunction, Biomaterials 285 (2022), 121541.
[46] K.H. Wrighton, Mitophagy turns beige adipocytes white, Nat. Rev. Mol. Cell Biol. 17 (2016) 607.